Argo profiles a rare occurrence of three consecutive positive Indian Ocean Dipole events, 2006–2008

W. Cai,[1,2] A. Pan,[3] D. Roemmich,[4] T. Cowan,[1,2] and X. Guo[3]

Received 16 December 2008; revised 11 March 2009; accepted 20 March 2009; published 16 April 2009.

[1] During 2006–2008, the Indian Ocean (IO) experienced a rare realization of three consecutive positive IO Dipoles (pIODs), including an unusual occurrence with a La Niña in 2007. Common to all three pIODs is an early excitation of equatorial easterly anomalies. Argo profiles reveal that for the 2008 and 2006 pIODs the wind anomalies are generated by the following process: upwelling Rossby waves propagating into the western IO and their subsequent reflection as equatorial upwelling Kelvin waves enhance the seasonal upwelling, changing sea surface temperature (SST) gradients. For the 2007 pIOD, coastal upwelling Kelvin waves off the Sumatra-Java coast associated with the 2006 pIOD/El Niño, radiate into the IO as upwelling Rossby waves. They curve sharply equatorward to arrive at the central equatorial IO, inducing easterly anomalies, upwelling Kelvin waves, and the unusual pIOD. Our results suggest that real-time Argo observations, when assimilated into predictive systems, will enhance IOD forecasting skills. **Citation:** Cai, W., A. Pan, D. Roemmich, T. Cowan, and X. Guo (2009), Argo profiles a rare occurrence of three consecutive positive Indian Ocean Dipole events, 2006–2008, *Geophys. Res. Lett.*, *36*, L08701, doi:10.1029/2008GL037038.

1. Introduction

[2] A pIOD event refers to a pattern of cool SST anomalies in the eastern IO and warm anomalies in the west. Such events are known to induce droughts in East Asia, Australia, and the Arabian Peninsula, and floods to parts of India and East Africa during austral winter and spring [*Saji et al.*, 1999; *Ashok et al.*, 2003; *Meyers et al.*, 2007]. Indeed, the 2006–2008 consecutive pIODs appeared to contribute to the prolonged current drought over southeastern Australia, surpassing the previously severest dry period of 1939–1946. In May 2008, observations showed the development of pIOD-conducive easterly anomalies over the equatorial IO (Figure 1, blue curve). By mid-June, a well-defined pIOD event was observed (Figure 2), leading to a rare occurrence of three consecutive pIODs. Moreover, the 2007 occurrence of a pIOD in a La Niña year was unique, although according to *Behera et al.* [2008], a pIOD and La Niña combination occurred in 1967.

[3] Although El Niño is a trigger of the IOD, other large-scale climate drivers also operate [*Saji et al.*, 2006], including the Southern Annular Mode and the onset of the Asia monsoon. Further, a Bjerknes-like positive feedback operates to generate an unstable growth of an initial perturbation regardless of its trigger. The feedback, involving anomalies of equatorial SST gradient, wind, and thermocline depth, works in such a way that the growth of one field reinforces that of other fields, as discussed in previous studies [e.g., *Saji et al.*, 1999]. The rare combination of a pIOD and a La Niña in 2007 provides unambiguous evidence for the IO's own capability to initiate and sustain a pIOD.

[4] These consecutive events are best observed with unprecedented predictive and observational capabilities that include Argo temperature/salinity profiling floats. Indeed, they were predicted [*Luo et al.*, 2008]. Mooring data near the eastern pole [*Horii et al.*, 2008] show that the surface signature of the 2006 pIOD was preceded by a thermocline signal some three months earlier. Using available surface observations and model outputs *Behera et al.* [2008] discuss the characteristics of wind anomalies and reveal a three-cell structure of the Walker circulation in the tropical Indo-Pacific system associated with the pIOD-La Niña combination (as opposed to the usual two-cell structure), highlighting that the pIOD is not triggered by the Pacific winds.

[5] Here we show that a commonality of the three events is a rapid development of easterly anomalies over the tropical IO in April/May. We then use Argo profiles to reveal that the precursory winds are preceded by thermocline anomalies that are consistent with a thermocline-SST coupling in the southwestern tropical IO and in the equatorial IO.

2. Data

[6] Quality controlled temperatures from Argo profiles, as described by *Roemmich and Gilson* [2009], are used to examine the relationship between anomalies of the thermocline and the precursory winds. The Argo profile data are mapped on a $1^\circ \times 1^\circ$ horizontal grid, with a vertical resolution ranging from 5m to 20m for the upper 400m. Temporal grid-spacing is 5 days, based on overlapping 10-day data collections. The thermocline depth (defined as the 20°C isotherm depth, D20) is calculated, and anomalies (both monthly and five-daily) are constructed based on the 2004–2007 climatology. To depict equatorial Kelvin waves, TOPEX/Poseidon sea surface height (SSH) data [*Le Traon et al.*, 1998] are analysed. Further, SSTs from the Tropical Rain Measuring Mission (TRMM) [*Wentz et al.*,

[1]CSIRO Marine and Atmospheric Research, Aspendale, Victoria, Australia.
[2]Wealth from Oceans National Research Flagship, CSIRO, North Ryde, New South Wales, Australia.
[3]Ocean Dynamics Laboratory in the Taiwan Strait and Tropical Marginal Sea, Third Institute of Oceanography, Xiamen, China.
[4]Scripps Institution of Oceanography, University of California, San Diego, La Jolla, California, USA.

0094-8276/09/2008GL037038$05.00

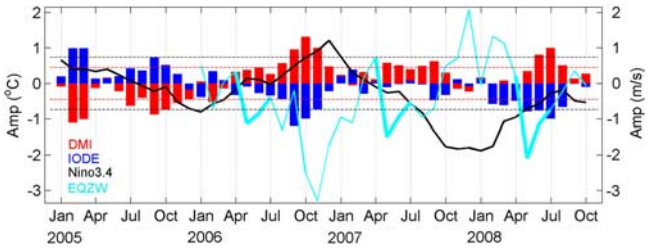

Figure 1. Time series of DMI (red bar, °C), SST anomalies averaged over IODE region (90°E–110°E and 10°S–0°N, blue bars, °C), Niño3.4 (SST anomalies averaged over 170°W–120°W, 5°S–5°N, black curve, °C), and EQZW anomalies averaged over the equatorial IO (50°E–100°E, 10°S–10°N, blue line, in m s^{-1}) with April and May portions highlighted. The red and black dashed lines represent the standard deviation of DMI (0.44°C) and Niño3.4 (0.75°C), respectively, based on the 2000–2007 period.

2000] from December 1998 onward, and surface winds from the QuikSCAT satellite scatterometer measurements [*Liu*, 2002] from July 1999 are utilized to describe the concurrent surface conditions. For these two fields, monthly and five-daily anomalies are derived from the climatological mean over 2000–2007, a period common to both data sets.

3. Commonalities of the Three Consecutive pIODs

[7] Common to all three pIOD events is an early development of the IO equatorial easterly anomalies (thickened blue, Figure 1). The role of easterly anomalies has been elucidated by previous studies [*Behera et al.*, 2006, 2008; *Luo et al.*, 2008]. Here we highlight features of these unusual events. The pan-equatorial IO average of equatorial zonal wind (EQZW) anomalies undergo a rapid growth from April to May before any sign of ENSO, as indicated by the small Niño3.4 in all three cases (black line, Figure 1).

[8] For the 2006 event, the easterly anomaly is followed by a rapid growth of cool SST anomalies in the eastern pole during the ensuing months. These anomalies are the principal contributor to the Dipole Mode Index (DMI; red bars, Figure 1), defined as the difference between SST anomalies averaged over a western and southeastern tropical IO (IODE; blue bars, Figure 1) box (west minus east [*Saji et al.*, 1999]). The EQZW appears to decrease during June–July, reflecting an eastward propagation of easterly anomalies out of the far western IO. This feature is seen in all three episodes. By August, the pIOD has grown to more than one standard deviation in size, but Niño3.4 is still less than 0.3°C. After September, the already active pIOD is strengthened by the El Niño-induced easterly anomalies, following the canonical IOD behaviour. Thus, although the 2006 pIOD occurs in an El Niño year, the trigger is not the El Niño SST pattern.

[9] A similar evolution is observed during April and July 2007, but the size of the May anomalies is greater. Although the development of the 2007 La Niña is more rapid than that of the 2006 El Niño, by July, Niño3.4 is still smaller than 0.6°C in amplitude. By August, the pIOD is already established and persisting despite the rapid growth of the La Niña. In contrast to the 2006 pIOD, the 2007 event features a western pole dominance (red bars, Figure 1), a smaller amplitude, and an earlier matured phase (in September). After October, the IO is under the full influence of the La Niña, with a strong negative correlation between winds over the equatorial IO and over the western Pacific. In short, an early commencement of strong easterly anomalies is again a key feature.

[10] The evolution of oceanic conditions during April-May 2008 resembles that of the 2007 event, but with the Pacific in a decaying La Niña phase. By mid-June, the DMI has reached one and half times the standard deviation value. This evolution again features an early development of easterly anomalies, which are even greater than the 2007 wind regime (see *Behera et al.* [2008] for a discussion of the 2007 case). Below we show that these wind anomalies are generated by ocean-atmosphere interactions within the IO sector.

4. Thermocline and Equatorial IO Easterly Anomalies

[11] We start with the 2008 pIOD event. The evolution and the spatial structure of the circulation anomalies during April–June (Figure 2) highlight the essential role of the equatorial precursory easterlies, consistent with previous studies [*Behera et al.*, 2006, 2008; *Luo et al.*, 2008]. By April, the easterlies are already present in the southwestern tropical IO, supported by consistent north–south SST gradients (Figure 2b). These easterlies belong to the northern branch of an anticyclonic circulation pattern that sits

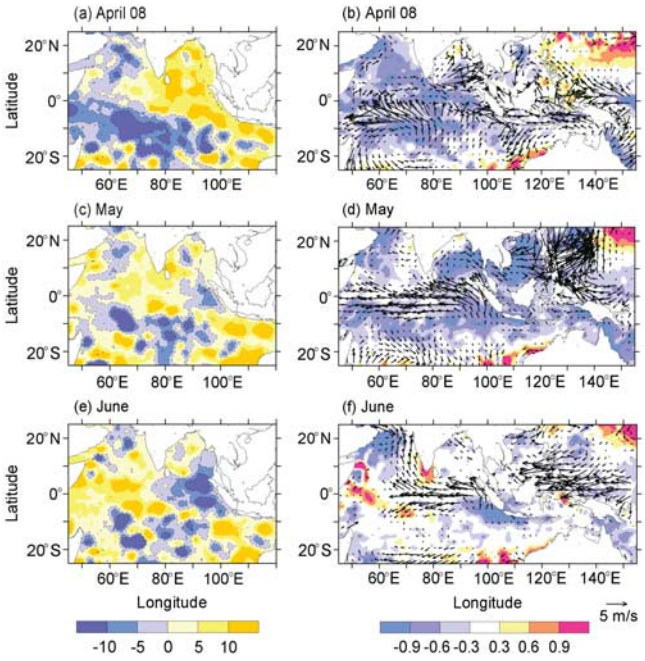

Figure 2. Development of the 2008 pIOD. (a) April 2008 anomalies of the thermocline depth from Argo (m). (b) April anomalies of TRMM SST (°C) and QuikSCAT winds (vectors in m s^{-1}). (c) Same as Figure 2a but for May. (d) Same as Figure 2b but for May. (e) Same as Figure 2a but for June. (f) Same as Figure 2b but for June.

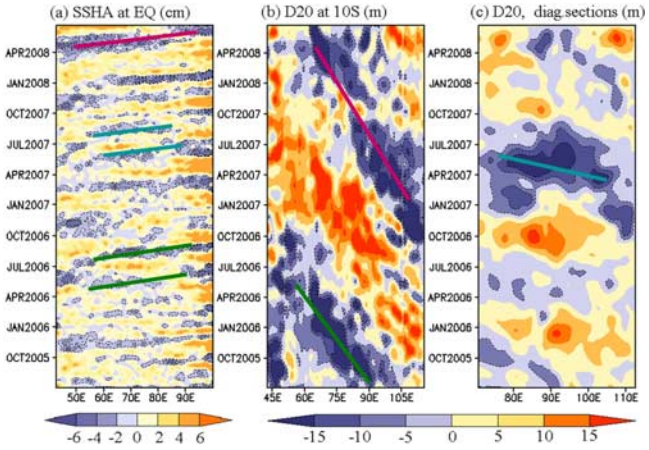

Figure 3. (a) Band passed SSH anomalies retaining signals on time scales between 20 days and 180 days. (b and c) Time longitude plot of D20 anomalies retaining signals on time scales longer than 60 days along 10°S and averaged over four sections bounded by the two dashed lines indicated in Figure 4a. In Figure 3c, the western end corresponds to the equator. Straight lines are drawn to indicate wave activities leading to pIOD development, pink for 2008, blue for 2007, green 2006.

over upwelling Rossby waves propagating westward along 10°S (Figures 2a and 3b) into the southwestern tropical IO thermocline dome, where a strong thermocline-SST coupling operates [*Xie et al.*, 2002; *Huang and Kinter*, 2002; *Rao and Behera*, 2005]. As Rossby waves propagate into the dome, an enhancement of the strong mean upwelling strengthens the surface cooling and the temperature gradient, which in turn reinforces the winds. In the subsequent months, a similar thermocline-SST coupling operates along the equator after the upwelling Rossby waves impinge on the western boundary and reflect as upwelling Kelvin waves (pink line, Figure 3a). The entire anomaly system then moves eastward into the eastern IO (Figures 2c–2f and 3a), where these anomalies grow further into a pIOD (Figure 2f).

[12] The easterly anomalies occur in the form of episodic wind bursts, as does the generation of equatorial Kelvin waves. The short time duration for equatorial Kelvin waves to traverse the IO, and the low spatial and temporal resolution of the Argo profiles make it a challenge to identify equatorial Kelvin waves within the data. Band-passed TOPEX/Poseidon SSH anomalies (Figure 3a) anomalies along the equator display clear episodic equatorial Kelvin waves that propagate eastward all year round, although only those during May–October are conducive to pIOD development (highlighted by straight lines in Figure 3a). For the 2008 pIOD, a strong Kelvin wave is generated subsequent to the reflection of upwelling Rossby waves (pink lines, Figures 3a and 3b). In summary, the genesis of easterly anomalies is oceanic Rossby waves and their coupling with SSTs in the thermocline dome and the equatorial region.

[13] What then generates the upwelling Rossby waves? Along 10°S, a well-defined biennial signal is apparent during 2006–2008 (Figure 3b). From October 2007 to March 2008, La Niña-induced westerly anomalies persist over the equatorial IO (Figure 1), consistent with the classic ENSO atmospheric teleconnection. It is the associated Ekman mass transport that drives the off-equatorial upwelling Rossby waves (pink line, Figure 3b). Likewise, the upwelling Rossby waves (green line, Figure 3b) during 2005–2006 are forced by westerly anomalies associated with the weak 2005/06 La Niña. Their western boundary reflection induces a series of equatorial Kelvin waves (green lines, Figure 3a), initiating the 2006 pIOD. Conversely, the downwelling Rossby waves during 2006–2007 are generated by equatorial easterly anomalies associated with the 2006 El Niño, which should lead to a negative IOD. Why doesn't this eventuate?

[14] After the demise of the 2006 pIOD, coastal upwelling Kelvin waves off the Sumatra/Java coast continue to be generated by El Niño-induced easterlies over the equatorial and eastern IO (figure not shown). By April 2007 (Figure 4a), Kelvin wave signals radiate into the IO as upwelling Rossby waves, which curve sharply equatorwards, faster when closer to the equator, bypassing the western boundary reflection. At the same time, off-equatorial downwelling Rossby waves propagate into the thermocline dome and impinge on the western boundary; this should generate westerlies through the thermocline-SST coupling. Westerly anomalies are indeed generated immediately south of the equator (Figure 4b). However, along the equator, weak easterly anomalies to the west and anomalous thermocline shallowing to the east are seen (Figures 4a and 4b). This is followed by a rapid growth of equatorial easterly anomalies with strong warming to the west (Figures 4c and 4d) as a consequence of the thermocline-SST coupling associated with the western boundary-reflected downwelling waves. The large warming in the west is an important differentiation of the 2007 pIOD from other events. To the east, continuous arrival of the equatorward-curving upwelling Rossby waves (Figure 4c) precedes a series of equatorial

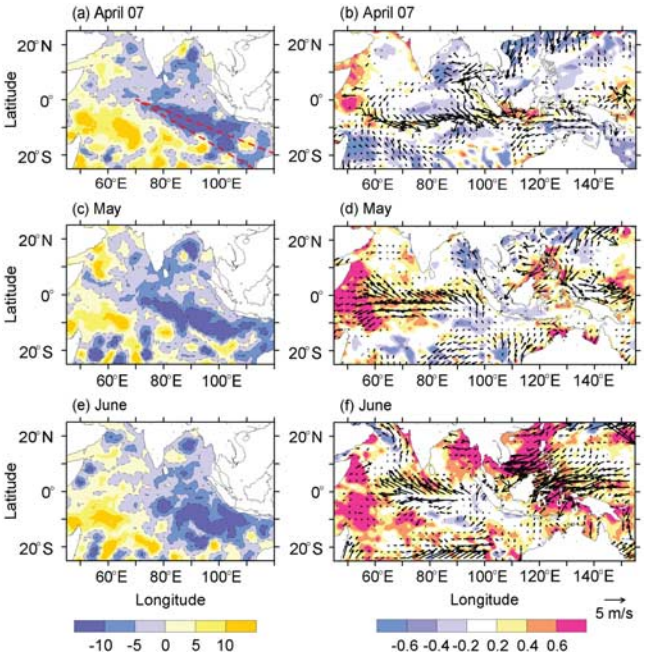

Figure 4. Same as Figure 2 but for 2007. Anomalies of D20 averaged over four sections bounded by the two red dashed lines are taken to construct Figure 3c.

upwelling Kelvin waves with little sign of western boundary origin (blue lines, Figure 3a), ahead of downwelling Kelvin waves reflected from the western boundary. This appears to trigger a Bjerknes-like positive feedback along the equator, and the entire anomaly system propagates toward the eastern IO (Figures 4e and 4f), leading to development of cold anomaly in the eastern IO in September (Figure 1).

[15] The feature of off-equatorial upwelling Rossby waves shortcutting to the equator is further highlighted in Figure 3c in a Hovemoller diagram of D20 anomalies averaged over four sections bounded by the two red dashed lines in Figure 4a. Rossby waves shortcutting to the equator are not uncommon. The extraordinary element in the 2007 case (blue line, Figure 3c) is their strength and arrival at the equator after May, i.e., during the pIOD favourable months. It is the continuous arrival of these upwelling Rossby waves that helps trigger easterly anomalies in May (Figure 4d), manifested as a stronger than normal southeasterly monsoon [*Behera et al.*, 2008]. Although wind stress curls appear favourable (Figure 4b) and reinforce the upwelling Rossby waves, further analysis is required to address why the shortcutting Rossby waves are able to acquire such strength during 2007. Thus, although with varying details, the precursory easterlies are preceded by thermocline anomalies, with a consistent oceanic and atmospheric feedback at play within the IO; the Pacific exerts no influence during this phase.

[16] The generation process of the 2006 pIOD (figure not shown) resembles that of the 2008 pIOD, involving off-equatorial upwelling Rossby waves passing through the thermocline dome. Under the influence of the thermocline-SST coupling these generate SST and easterly wind anomalies, inducing the pIOD by June, when the Pacific still shows no sign of an El Niño developing.

5. Discussion and Conclusions

[17] Common to the three consecutive pIODs is an early development in April/May of equatorial easterly anomalies, which induce and reinforce eastward propagating Kelvin waves into to the eastern IO. The precursory easterly anomalies, once generated, become an active participant of the Bjerknes-like feedback and undergo a rapid growth involving anomalies of SST gradients and thermocline depth. In all three events, the trigger of easterly anomalies appears to reside in the interior IO, commencing in southern tropical IO and then moving to the equator. Although the interior IO anomalies may be linked to ENSO teleconnection months earlier, the evolution after April/May is internal to the IO.

[18] Argo and other observations reveal that for the 2008 and 2006 pIODs the easterly anomalies are preceded by the following oceanic process: upwelling Rossby waves propagating through the IO thermocline dome and their subsequent reflection as equatorial upwelling Kelvin waves enhance the seasonal upwelling, thereby changing SST gradients and giving rise to the easterly anomalies. For the 2007 pIOD, coastal upwelling Kelvin waves off the Sumatra-Java coast associated with the 2006 pIOD/El Niño, radiate into the IO as upwelling Rossby waves. As they move westward, they curve equatorward, bypassing the western boundary to arrive at the central equatorial IO ahead of downwelling Kelvin waves reflected from the western boundary. This triggers a Bjerknes-like positive feedback along the equator, leading to the unusual pIOD event.

[19] That these precursory easterly anomalies are preceded by thermocline anomalies has important implications. It suggests that real-time Argo observations, when assimilated into predictive systems, will improve IOD prediction skills. The fact that these three consecutive events are predicted using SSTs alone [*Luo et al.*, 2008] highlights the robustness of the ocean-atmosphere coupling within the IO and suggests that by using Argo to provide the ocean memory, such coupling may be further exploited to improve IOD predictions.

[20] **Acknowledgments.** The Argo data used here were collected and are made freely available by the International Argo Program and by the national programs that contribute to it. A. Pan is supported by the National Basic Research Program of China (2007CB816002), Basic Scientific Research Foundation (2007018). W. Cai and T. Cowan are supported by the Australian Department of Climate Change. D. Roemmich was supported by NOAA grant NA17RJ1231 (U.S. Argo).

References

Ashok, K., Z. Guan, and T. Yamagata (2003), Influence of the Indian Ocean Dipole on the Australian winter rainfall, *Geophys. Res. Lett.*, *30*(15), 1821, doi:10.1029/2003GL017926.

Behera, S., J. Luo, S. Masson, S. Rao, H. Sakuma, and T. Yamagata (2006), A CGCM study on the interaction between IOD and ENSO, *J. Clim.*, *19*, 1688–1705.

Behera, S. K., J.-J. Luo, and T. Yamagata (2008), Unusual IOD event of 2007, *Geophys. Res. Lett.*, *35*, L14S11, doi:10.1029/2008GL034122.

Horii, T., H. Hase, I. Ueki, and Y. Masumoto (2008), Oceanic precondition and evolution of the 2006 Indian Ocean dipole, *Geophys. Res. Lett.*, *35*, L03607, doi:10.1029/2007GL032464.

Huang, B., and J. L. Kinter III (2002), Interannual variability in the tropical Indian Ocean, *J. Geophys. Res.*, *107*(C11), 3199, doi:10.1029/2001JC001278.

Le Traon, P. Y., F. Nadal, and N. Ducet (1998), An improved mapping method of multisatellite altimeter data, *J. Atmos. Oceanic Technol.*, *15*, 522–533.

Liu, W. T. (2002), Progress in scatterometer application, *J. Oceanogr.*, *58*, 121–136.

Luo, J.-J., S. Behera, Y. Masumoto, H. Sakuma, and T. Yamagata (2008), Successful prediction of the consecutive IOD in 2006 and 2007, *Geophys. Res. Lett.*, *35*, L14S02, doi:10.1029/2007GL032793.

Meyers, G. A., P. C. McIntosh, L. Pigot, and M. J. Pook (2007), The years of El Niño, La Niña, and interactions with the tropical Indian Ocean, *J. Clim.*, *20*, 2872–2880.

Rao, S. A., and S. K. Behera (2005), Subsurface influence on SST in the tropical Indian Ocean: structure and interannual variability, *Dyn. Atmos. Ocean*, *39*, 103–135.

Roemmich, D., and J. Gilson (2009), The 2004–2007 mean and annual cycle of temperature, salinity and steric height in the global ocean from Argo Program, *Prog. Oceanogr.*, in press.

Saji, N. H., B. N. Goswami, P. N. Vinayachandran, and T. Yamagata (1999), A dipole mode in the tropical Indian Ocean, *Nature*, *401*, 360–363.

Saji, N. H., S.-P. Xie, and T. Yamagata (2006), Tropical Indian Ocean variability in the IPCC twentieth-century climate simulations, *J. Clim.*, *19*, 4397–4417.

Wentz, F. J., C. Gentemann, D. Smith, and D. Chelton (2000), Satellite measurements of sea surface temperature through clouds, *Science*, *288*, 847–850.

Xie, P., F. A. Schoot, and J. P. McCreary Jr. (2002), Structure and mechanism of South Indian Ocean climate variability, *J. Clim.*, *15*, 864–878.

W. Cai and T. Cowan, CSIRO Marine and Atmospheric Research, PMB 1, Aspendale, Vic 3195, Australia. (wenju.cai@csiro.au)

X. Guo and A. Pan, Ocean Dynamics Laboratory in the Taiwan Strait and Tropical Marginal Sea, Third Institute of Oceanography, 178 Daxue Road, P.O. Box 0570, Xiamen, Fujian 361006, China.

D. Roemmich, Scripps Institution of Oceanography, University of California, San Diego, 9500 Gilman Drive, La Jolla, CA 92093-0230, USA.